Optical characterisation of plasmonic nanostructures on planar substrates using second–harmonic generation

Lina Persechini,[1,*] Ruggero Verre,[1,2] Christopher M. Smith,[1] Karsten Fleischer,[1,2] Igor V. Shvets,[1,2] Mukesh Ranjan,[3,4] Stefan Facsko,[4] and John F. McGilp[1]

[1]*School of Physics, Trinity College Dublin, Dublin 2, Ireland*
[2]*Centre for Research on Adaptive Nanostructures and Nanodevices (CRANN), Trinity College Dublin, Dublin 2, Ireland*
[3] *FCIPT, Institute for Plasma Research, Gandhinagar, India*
[4] *Institute of Ion Beam Physics and Materials Research, Helmholtz–Zentrum Dresden–Rossendorf, 01314 Dresden, Germany*
[*]*persechl@tcd.ie*

Abstract: Off-normal, polarization dependent second–harmonic generation (SHG) measurements were performed *ex situ* on plasmonic nanostructures grown by self–assembly on nanopatterned templates. These exploratory studies of Ag nanoparticle (NP) arrays show that the sensitivity of SHG to the local fields, which are modified by the NP size, shape and distribution, makes it a promising fixed wavelength characterization technique that avoids the complexity of spectroscopic SHG. The off–normal geometry provides access to the out–of–plane SH response, which is typically an order-of-magnitude larger than the in–surface–plane response measured using normal incidence, for example in SHG microscopy. By choosing the plane of incidence orthogonal to the NP array direction, it was shown that the $p-$polarized SH response, as a function of input polarization, is very sensitive to NP morphology, with a change of 20% in the aspect ratio of the NPs producing a variation of a factor of 30 in the easily measureable ratio of the $p-$polarized SH field strength for $s-$ and $p-$polarized input. The results show that such a fixed geometry could be used for the *in situ* characterization of anisotropic nanostructure morphology during growth by self–assembly, which could be particularly useful in situations where rotating the sample may be neither desirable nor easily accomplished.

OCIS codes: (190.4350) Nonlinear optics at surfaces; (190.4400) Nonlinear optics, materials; (240.6680) Surface plasmons.

References and links

1. U. Kreibig and M. Vollmer, "*Optical Properties of Metal Clusters*" (Springer, 1995).
2. S. A. Maier and P.G. Kik and H. A. Atwater and S. Meltzer and E. Harel and B. E. Koel and A. A. G. Requicha, "Local detection of electromagnetic energy transport below the diffraction limit in metal nanoparticle plasmon waveguides," Nature Mater. **2**, 229–232 (2003).
3. P. K. Jain and X. Huang and I. H. El-Sayed and M. A. El-Sayed, "Review of some interesting surface plasmon resonance–enhanced properties of noble metal nanoparticles and their applications to biosystems," Plasmonics **2**, 107–118 (2007).

#243962 Received 8 Jul 2015; revised 25 Sep 2015; accepted 26 Sep 2015; published 1 Oct 2015

4. H. A. Atwater and A. Polman, "Plasmonics for improved photovoltaic devices," Nature Mater. **9**, 205–213 (2010).
5. B. Sharma B and R. R. Frontiera and A. I. Henry and E. Ringe andR. P. Van Duyne, "SERS: materials, applications, and the future," Mater. Today **15**, 16–25 (2012).
6. S. Camelio and D. Babonneau and D. Lantiat and L. Simonot, "Self–organized growth and optical properties of silver nanoparticle chains and stripes," Europhys. Lett. **79**, (2007).
7. R. Verre and K. Fleischer and J. F. McGilp and D. Fox and G. Behan and H. Zhang and I. V. Shvets, "Controlled *in situ* growth of tunable plasmonic self–assembled nanoparticle arrays," Nanotechnology **23**, 035606 (2012).
8. A. Keller and S. Facsko S, "Ion-Induced Nanoscale Ripple Patterns on Si Surfaces: Theory and Experiment," Materials **3**, 4811–4841 (2010).
9. A. Toma and D. Chiappe and C. Boragno and F. Buatier de Mongeot, "Self-organized ion-beam synthesis of nanowires with broadband plasmonic functionality," Phys. Rev. B **81**, 165436 (2010).
10. S. J. Chey and J. E. Van Nostrand and D. G. Cahill, "Surface morphology of Ge(001) during etching by low–energy ions," Phys. Rev. B **52**, 16696–16701 (1995).
11. W. L. Chan and E. Chason, "Making waves: kinetic processes controlling surface evolution during low energy ion sputtering," J. Appl. Phys. **101**, 121301 (2007).
12. R. M. Bradley and J. M E. Harper, "Theory of ripple topography induced by ion bombardment," J. Vac. Sci. Technol. A **6**, 2390–2395 (1988).
13. S. Camelio and E. Vandenhecke and S. Rousselet and D. Babonneau, "Optimization of growth and ordering of Ag nanoparticle arrays on ripple patterned alumina surfaces for strong plasmonic coupling," Nanotechnology **25**, 035706 (2014).
14. S. Rusponi and G. Costantini and C. Boragno and U. Valbusa, "Ripple wave vector rotation in anisotropic crystal sputtering," Phys. Rev. Lett. **81**, 2735–2738 (1998).
15. J. F. McGlip, "Optical characterisation of semiconductor surfaces and interfaces," Prog. Surf. Sci. **49**,1–106 (1995).
16. R. Verre and K. Fleischer and R. G. S. Sofin and N. McAlinden and J. F. McGilp and I. V. Shvets, "*In situ* characterization of one–dimensional plasmonic Ag nanocluster arrays," Phys. Rev. B. **83**, (2011).
17. R. Verre and K. Fleischer and C. Smith and N. McAlinden and J. F. McGilp and I. V. Shvets, "Probing the out-of-plane optical response of plasmonic nanostructures using spectroscopic ellipsometry," Phys. Rev. B. **84**, 085440 (2011).
18. L. Persechini and R. Verre and N. McAlinden and J. J. Wang and M. Ranjan and S. Facsko and I. V. Shvets and J. F. McGilp, "An analytic approach to modeling the optical response of anisotropic nanoparticle arrays at surfaces and interfaces," J. Phys. Condens. Matter **26**, 145302 (2014).
19. J. Butet and B. Gallinet and K. Thyagarajan and J. F. O. Martin, "Second-harmonic generation from periodic arrays of arbitrary shape plasmonic nanostructures: a surface integral approach," J. Opt. Soc. Am. B **30**, 2970–2979 (2013).
20. V. K. Valev, "Characterization of Nanostructured Plasmonic surfaces with second harmonic generation," Langmuir **28**, 15454–15471 (2012).
21. A. Belardini and M. C. Larciprete and M. Centini and E. Fazio E and C. Sibilia and M. Bertolotti and A.Toma and D. Chiappe and F. Buatier De Mongeot, "Tailored second-harmonic generation from self-organized metal nano-wires arrays," Opt. Exp. **17**, 3603–3609 (2009).
22. M. L. Ren and S. Y. Liu and B. L. Wang and B. Q. Chen and J. Li and Z. Y. Li, "Giant enhancement of second harmonic generation by engineering double plasmonic resonances at nanoscale," Opt. Express **22**, 28653–28661 (2014).
23. B. K. Canfield and S. Kujala and K. Jefimovs and T. Vallius and J. Turunen and M. Kauranen, "Polarization effects in the linear and nonlinear optical responses of gold nanoparticle arrays," J. Opt. A:Pure Appl. Op. **7**, S110 (2005).
24. B. K. Canfield and H. Husu and J. Laukkanen and B. Bai and M. Kuittinen and J. Turunen and M. Kauranen,"Local field asymmetry drives second-harmonic generation in noncentrosymmetric nanodimers," Nano Lett. **7**, 1251–1255 (2007).
25. C. Hubert and L. Billot and P. M. Adam and R. Bachelot and P. Royer and J. Grand and D. Gindre and K. D. Dorkenoo and A. Fort, "Role of surface plasmon in second harmonic generation from gold nanorods," Appl. Phys. Lett. **90**, 181105 (2007).
26. J. Butet and K. Thyagarajan and O. J. F. Martin,"Ultrasensitive optical shape characterization of gold nanoantennas using second harmonic generation," Nano Lett. **13**, 1787–1792 (2013).
27. C. Sauerbeck and M. Haderlein and B. Schürer and B. Braunschweig and W.Peuker and R. N. K. Taylor, "Shedding light on the growth of gold nanoshells," ACS Nano **8**, 3088–3096 (2014).
28. G. Luepke, "Characterization of semiconductor interfaces by second-harmonic generation," Surf. Sci. Rep. **35**, 3–4 (1999).
29. R. Verre and M. Modreanu and O. Ualibek and D. Fox and K. Fleischer and C. Smith and H. Zhang and M. Pemble and J. F. McGilp and I. V. Shvets, "General approach to the analysis of plasmonic structures using spectroscopic ellipsometry," Phys. Rev. B.**87**, 235428 (2013).
30. T. W. H. Oates and A. Keller and S. Facsko and S. Mücklich, "Aligned silver nanoparticles on rippled silicon

#243962 Received 8 Jul 2015; revised 25 Sep 2015; accepted 26 Sep 2015; published 1 Oct 2015

templates exhibiting anisotropic plasmon absorption," Plasmonics **2**, 47–50 (2007).
31. M. Ranjan and S. Facsko, "Anisotropic surface enhanced Raman scattering in nanoparticle and nanowire arrays," Nanotechnology **23**, 485307 (2012).
32. M. Ranjan and S. Facsko and M. Fritzsche and S. Mukherjee, "Plasmon resonance tuning in Ag nanoparticles arrays grown on ripple patterned templates," Microelectron. Eng. **102**, 44–47 (2013).
33. A. V. Zayats and I. I. Smolyaninov and A. A. Maradudin, "Nano-optics of surface plasmon polaritons," Phys. Rep. **408**, 131–314 (2005).
34. G. Bachelier and J. Butet and I. Russier-Antoine and C. Jonin and E.Benichou and P. F. Brevet, "Origin of optical second-harmonic generation in spherical gold nanoparticles: local surface and nonlocal bulk contributions," Phys. Rev. B. **82**, 235403 (2010)
35. J. R. Power and J. D. O'Mahony and S. Chandola and J. F. McGilp, "Resonant optical second–harmonic generation at the steps of vicinal Si(001)," Phys. Rev. Lett. **75**, 1138–1141 (1995).
36. J. Jacob and A. G. Silva and K. Fleischer and J. F. McGilp,"Optical second–harmonic generation studies of Si(111)- $\sqrt{3}\times\sqrt{3}$-Ag and Si(111)-3×1-Ag grown on vicinal Si(111)," Phys. Status Solidi C. **5**, 2649–2652 (2008).
37. L. Persechini and M. Ranjan and F. Grossmann and S. Facsko and J. F. McGilp, "The linear and nonlinear optical response of native–oxide covered rippled Si templates with nanoscale periodicity," Phys. Status Solidi B. **249**, 1173–1177 (2012).

1. Introduction

Plasmonic nanostructures are being used as building blocks for a variety of nanophotonics applications. When metal nanoparticles (NPs) are illuminated, localized surface plasmon resonances (LSPRs) are excited, which are extremely sensitive to interactions with the environment. If several NPs are located in close proximity to one another, such that their induced evanescent fields overlap, the interactions can be so strong that the time varying charge distribution and the associated spectral response of the system will differ drastically from that of the isolated constituents [1]. Optical interactions between plasmonic NPs can produce many new phenomena, including strong local field enhancement, broadened spectral response and directional emission, which can be utilized for numerous applications, including waveguiding [2], biosensing [3] and improving the efficiency of solar cells [4]. The dramatic amplification of the optical response has also led to the development of LSP–enhanced spectroscopies, such as a variation of surface enhanced Raman scattering (SERS) that allows single molecule detection [5].

For these enhancement effects, strong coupling between nanoparticles is desired and the required length scales are challenging for conventional lithographic techniques, especially if large patterned areas are required. In these cases, self-assembly methods are an attractive alternative solution. Recently, an experimental approach for producing strongly coupled, aligned NP arrays in a reproducible fashion was developed by a number of groups, using similar methodologies based on glancing angle deposition on patterned templates. For example, the controlled annealing of vicinal single crystal Al_2O_3 substrates leads to faceted templates, which can be adjusted to control the periodicity and the growth of aligned nanoparticle (NP) arrays [6, 7]. Alternatively, low energy ion beam irradiation can produce self-organized, nanoscale periodic patterns on various solid substrates [8–14]. NPs deposited on such templates align themselves with respect to the ripple or facet direction, as shown in Fig. 1.

Monitoring the formation, in real time, of nanostructured templates and the evolution of NP arrays during growth, in order to ensure the required functionality, is challenging. Surface and interface sensitive optical techniques offer advantages in this area over conventional surface science techniques. Specifically, all pressure ranges of gas–solid interfaces are accessible, the material damage and contamination associated with charged particle probes is eliminated, and insulating substrates can be studied without the problem of charging effects [15]. For example, it has been shown recently that reflection anisotropy spectroscopy (RAS), a surface sensitive form of polarized reflectance, is a particularly useful *in situ* probe of Ag NP growth on faceted Al_2O_3 [7,16], while spectroscopic ellipsometry combined with analytic modelling of the optical

#243962 Received 8 Jul 2015; revised 25 Sep 2015; accepted 26 Sep 2015; published 1 Oct 2015

response also appears promising [17, 18].

The linear optical properties of such NP arrays and plasmonic nanostructures are now well understood. Progress is also being made in modelling the more complex nonlinear optical response, particularly regarding the enhancement effects of local fields and the sensitivity of second–harmonic generation (SHG) to NP shape [19]. The experimental characterization of plasmonic nanostructures using SHG has been reviewed recently, with an emphasis on SHG microscopy [20]. Other experimental work has explored methods of increasing the size of the SHG response from nanostructured arrays [21, 22]. Most of the characterization work has used normal incidence excitation. While this restricts the SHG response to the smaller in-surface-plane tensor components, polarization-dependent studies at normal incidence have been shown to be very sensitive to NP morphology [23–26].

The potential of SHG for monitoring the growth of anisotropic NP arrays appears to be largely unexplored. In a very recent study, the seeded growth of Au nanoshells in solution showed significant changes in the SHG response as the reaction proceeded [27]. In this paper, it is shown that polarization–dependent, off–normal–incidence measurements, which can access both the in-surface-plane and the larger out-of-surface-plane SHG tensor components [28], allow a simple non–resonant, fixed wavelength approach, compatible with *in situ* growth monitoring, to be used for characterizing NP morphology. The systems explored are Ag NPs grown on faceted Al_2O_3 and rippled Si(001).

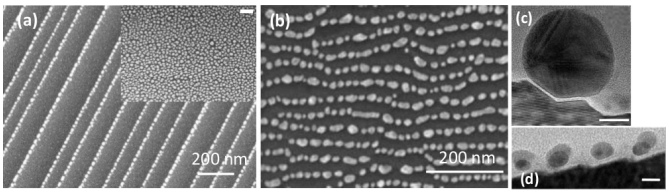

Fig. 1. (a) SEM image of Ag clusters on faceted Al_2O_3. Inset: SEM image of Ag clusters on unannealed Al_2O_3, where the Ag is deposited perpendicularly to the sample surface (scale bar 100 nm). (b) SEM image of Ag clusters on rippled Si(001) prior to capping with amorphous Si. (c) High magnification cross–sectional TEM image of Ag along the step edge of a faceted template, with an 8 nm scale bar (after [29]). (d) Cross–sectional TEM image of Ag NPs on a native–oxide–covered rippled Si substrate, with a 20 nm scale bar (after [30]). The larger particles are located in the ripple valleys.

2. Experiment

Anisotropic Ag nanostructures were grown by self–assembly using two techniques on different substrates. The Ag/Al_2O_3 system was produced by glancing angle deposition of Ag, using a technique described by Verre *et al* [16, 17], on vicinal α–Al_2O_3 under high vacuum conditions (base pressure of 2×10^{-8} mbar). The sapphire substrate is annealed for 24 hours at 1400°C, producing an ordered and faceted structure. The substrate is then tilted relative to a collimated Ag flux, resulting in arrays of anisotropic Ag NPs decorating the facets [Fig. 1(a)], and strong plasmonic resonances. The dimensions of the NPs were characterised using SEM and TEM, and the average NP size was 18 nm $\times$ 15 nm $\times$ 12 nm.

Ag islands on rippled nanostructures on a Si(001) substrate were grown under high vacuum conditions at the Helmholtz–Zentrum Dresden–Rossendorf, using a procedure that has been described in detail previously [31, 32]. The rippled structures have a nanoscale periodicity of 30 nm and an amplitude of $\sim$1 nm, as measured by AFM. The templates were prepared by irradiating native–oxide–covered Si(001) at room temperature with a collimated beam of 500 eV

#243962 Received 8 Jul 2015; revised 25 Sep 2015; accepted 26 Sep 2015; published 1 Oct 2015

Ar^+ ions at incidence angle of 67° with respect to the surface normal, aligned with the ⟨100⟩ azimuth. After *ex situ* characterization, Ag was deposited orthogonally to the ripples on the native–oxide–covered surface by electron beam evaporation at a grazing angle of 70° to the surface normal. SEM was used to characterize the Ag NP layer structure and Table 1 shows the average dimensions and island separations for the samples under investigation. Finally, a capping layer of 20 nm of amorphous silicon (*a*–Si) was deposited to limit tarnishing of the NPs. The penetration depth of the optical probe allows the NP layer to be characterized through the capping layer. Figures 1(c) and 1(d) show cross–sectional TEM images of the NP layers. It can be seen that the Ag NPs are separated from the substrates by ∼1 nm, due to the native oxide layer in the case of rippled Si, and the tarnishing of the uncapped Ag NPs on the faceted Al_2O_3.

Optical measurements of Ag NPs on rippled Si and Al_2O_3, were performed in ambient conditions. Measurements on Ag on rippled Si substrates were reproducible after several months, due to the protection of the capping layer, unlike the Ag on Al_2O_3 samples, where experiments were performed within hours of exposure to ambient in order to reduce the effects of tarnishing of the NP layer on the SH response. The SHG measurements were made in reflection using a femtosecond laser tuned to a wavelength of 800 nm. Unamplified 130 fs Ti:sapphire laser pulses of an average power of 200 mW at the samples were used, at a repitition rate of 76 MHz. An off–normal geometry was chosen to allow access to the p–polarized SH response, which involves the larger out–of–plane tensor components, [28]. The input beam of 60 μm diameter at the sample was incident at 45°. A half–wave plate in the input beam was used to rotate the polarization vector of the linearly polarized light and the *p*– and *s*–polarized SH responses were measured as a function of wave plate angle, using a Pellin–Broca prism to spatially separate the SH beam from the fundamental. The diode–pumped laser system is very stable and it was sufficient to normalise the signal using the square of the laser output power.

Table 1. Average dimensions of Ag NP structure on Al_2O_3 and rippled Si obtained from analysis of SEM images. S1, S2 and S3 are *a*–Si/Ag/rippled Si(001). The centre–to–centre NP distances along and across the islands are given by l_y and l_x, respectively. Estimated errors in parenthesis provide a guide to the variation in dimensions.

Sample	y **nm**	x **nm**	**Aspect ratio**	l_y **nm**	l_x **nm**	**NP density** 10^{15} **m**$^{-2}$
Ag/flat Al_2O_3	15(4)	15(4)	1	30(11)	26(7)	3.0(3)
Ag/Al_2O_3	18(5)	15(3)	1.20	24(6)	120(35)	0.65(4)
S1	28(10)	16(3)	1.75	34(7)	30(4)	1.1(2)
S2	24(9)	15(3)	1.60	29(7)	30(4)	1.1(2)
S3	22(7)	15(3)	1.47	27(4)	29(6)	1.4(2)

3. Theory and SHG phenomenology

In general, local fields at interfaces increase the intensity of the SHG response by a factor of $\left|L(2\omega)L^2(\omega)\right|^2$ [33], where $L(\omega)$ and $L(2\omega)$ are the field enhancement factors at the fundamental and SH wavelengths, respectively. $L(\omega) \sim |E_{loc}/E_0|$, where E_{loc} is the local field and E_0 is the incident field. The plasmonic structures enhance nonlinear effects by local field enhancement, near the metal–dielectric interface, associated with the excitation of LSPs.

Nonlinear effects are governed by the symmetry of the material. Within the electric dipole approximation, SHG is forbidden in the bulk of a centrosymmetric material and it is the breaking of symmetry at the interface of such materials that makes SHG surface and interface sensitive. For NPs located at the interface between centrosymmetric materials, a SH response is

#243962 Received 8 Jul 2015; revised 25 Sep 2015; accepted 26 Sep 2015; published 1 Oct 2015

expected due to the reduced symmetry of the local fields acting on the NP surface response, the non-local bulk response from centrosymmetric metallic NPs being much smaller [34]. For the experimental approach used here, the variation of the $s-$ and $p-$polarized SH intensity is of the form,

$$I_p^{\alpha} \propto |A\cos^2\alpha + B\sin^2\alpha + C\sin 2\alpha|^2 \quad (1)$$

$$I_s^{\alpha} \propto |F\cos^2\alpha + G\sin^2\alpha + H\sin 2\alpha|^2 \quad (2)$$

where α is the polarization vector angle of the linearly polarized light with respect to the plane of incidence [15]. The SH response is fitted to Eqs. (1) and (2), by varying A to H, which will be complex when the exciting field or the SH field is close to a resonance of the system. These phenomenological parameters depend on Fresnel coefficients and the dipolar second order susceptibility tensor components $\chi^{(2)}_{ijk}$. Higher order terms, arising from the bulk quadrupolar contribution and the effects of strain and static electric fields may also contribute to a smaller extent to the response [28]. The presence of symmetry elements at the interface reduces the number

Table 2. Allowed tensor components for each parameter, assuming no symmetry elements, for α-p and α-s measurements

Parameter	χ_{ijk} (*xz* plane)	χ_{ijk} (*yz* plane)
A	zxx zxz zzz	zyy zyz zzz
	xxx xzz	yyy yzy yzz
B	zyy xyy	zxx yxx
C	zxy zyz	zyx zxz
	xyx xyz	yxy yxz
F	yxx yxz yzz	xyy xyz xzz
G	yyy	xxx
H	yxy yzy	xyx xzx

of independent tensor components, but the data were fitted assuming no symmetry. The allowed tensor components according to each parameter are shown in Table 2. For a $p-$polarized output, A corresponds to a pP geometry and B corresponds to an sP geometry, where the first and second letters refer to the input and output polarizations, respectively. For an $s-$polarized output, F corresponds to pS and G corresponds to sS.

Measurements were made with the plane of incidence along the NP array (*yz* plane, *y*–azimuth) and across the NP array (*xz* plane, *x*–azimuth), as shown in Fig. 2. The presence of any symmetry elements at the interface will simplify the response. For example, the allowed electric dipole ijk terms are zzz, $zxx = zyy$, and $xzx = yzy$ for a Si(001) interface with 4mm symmetry. For the $s-$polarized output, Table 2 shows that only H contributes *via* the $xzx = yzy$ component, resulting in a simple $\sin^2(2\alpha)$ behaviour for this high symmetry interface. More generally, if the plane of incidence is a mirror plane of the interface, then only H contributes to the $s-$polarized SH response [35].

4. Results and discussion

Selected samples were analysed using linear optics to assess reflectivities and resonance energies: some of these results have been published elsewhere [18]. SHG was then performed: α–p and α–s measurements were made on Ag on Al_2O_3 and on rippled Si samples, along both *x*– and *y*–azimuths.

#243962 Received 8 Jul 2015; revised 25 Sep 2015; accepted 26 Sep 2015; published 1 Oct 2015

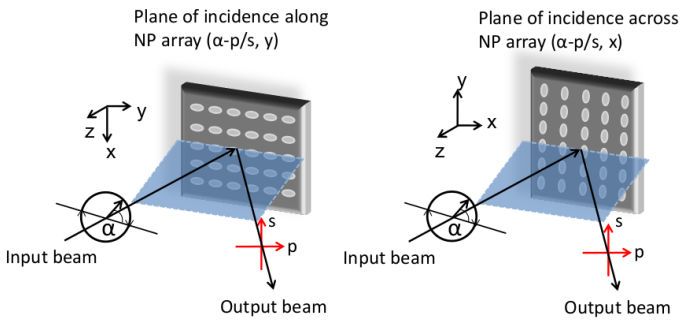

Fig. 2. Geometry of SHG measurements, where the polarization vector of the input beam is rotated and either the *s*– or *p*–polarized SH intensity is measured. The plane of incidence is aligned either along (*y*–azimuth) or across (*x*–azimuth) the NP arrays.

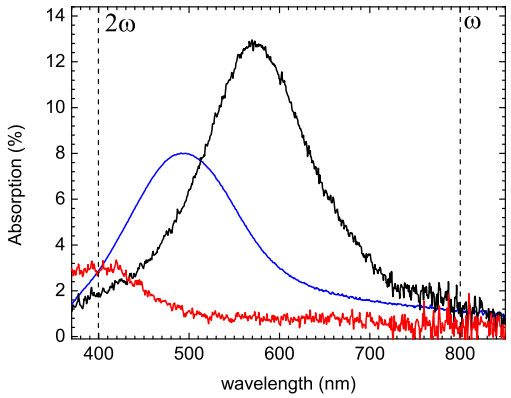

Fig. 3. Absorbance spectra of Ag NPs arrays [Fig. 1(a)] on flat and faceted alumina probed by spectrophotometry. A correction was applied to the UV region of the spectrum to eliminate an increased background signal due to scattering. Polarization dependent absorbance parallel (black line) and perpendicular (red line) to the islands on faceted Al_2O_3 is shown. The response from Ag islands on flat Al_2O_3 (blue line) is also shown. The fundamental and SH wavelengths are marked on the figure.

4.1. Ag on Al_2O_3

The polarized absorbance spectra from Ag on flat and on faceted Al_2O_3 are shown in Fig. 3, where a correction has been applied in the UV region to account for a monotonically increasing background signal due to scattering. Polarization dependent absorbance features are observed when the electromagnetic field is aligned parallel and perpendicular to the NP array. The LSPRs along the arrays (*y*–azimuth) appear in the visible range, where the difference in peak width and position is due to island separation, shape, and shape dispersion. The figure also shows that the fundamental wavelength is off–resonance, while any resonance enhancement at the SH wavelength is likely to be small.

4.1.1. Ag on flat Al_2O_3:

Figure 4 shows polar plots of the α–p and α–s response measured along each azimuth. The response of the uncoated surface was negligible under these conditions, and so the measured

#243962 Received 8 Jul 2015; revised 25 Sep 2015; accepted 26 Sep 2015; published 1 Oct 2015

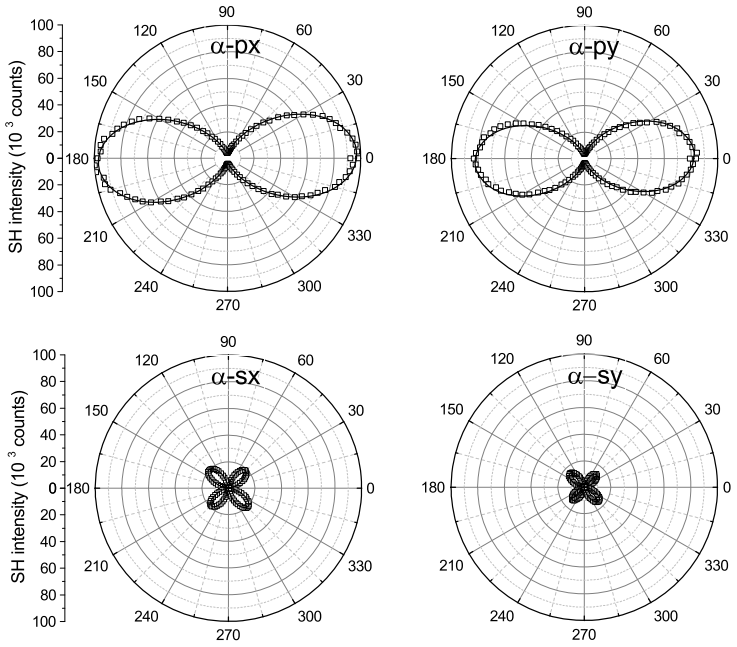

Fig. 4. α–p and α–s SH response plotted as a function of polarizer angle in both azimuths, for Ag NPs on flat Al_2O_3, together with fits (black line) using Eqs. 1 and 2

SHG response is due entirely to the NP layer. The signal is approximately an order of magnitude larger than that from native-oxide-covered silicon using 800 nm excitation, and is easily detected. The size of the response is also comparable for the NP arrays on the rippled Si substrates (see later), indicating that the SHG response from NP arrays grown on semiconductor and insulating substrates can be easily detected using non–resonant conditions. The inset in Fig. 1(a) shows that deposition of Ag on a flat substrate produces more symmetric NPs and does not result in the formation of NP arrays. We observe very similar lineshapes from both azimuths, consistent with the roughly isotropic distribution of NP shapes and arrangement on the surface. Table 3 shows the parameter values extracted from the fits. Both the figure and the table show that the two azimuths are very similar. For the α–s response, there is a very small departure from the $\sin^2(2\alpha)$ behaviour (lobes of equal intensity at 45° and related angles) that would be expected if the NP distribution were fully isotropic. Some of this departure arises from a slight imperfection in the half–wave plate and its sensitivity to alignment, which has been discussed in a previous publication [36], however the small but significant difference between the azimuths of the α–s response, and also in the A parameter value of the α–p response (Table 3), shows that a very small anisotropy in the NP growth on flat Al_2O_3 cannot be ruled out. As well as confirming the largely isotropic NP morphology, Fig. 4 shows that the $p-$polarized SH response, which is accessible when an off–normal geometry is used, is roughly an order–of–magnitude larger than the $s-$polarized response. It is well known that $p-$polarization, which accesses out–of–plane, $z-$dependent tensor components, produces a much larger SH response at interfaces [28], with the maximum signal generally being obtained for the pP configuration ($\alpha = 0^\circ$), as seen in Fig. 4.

#243962 Received 8 Jul 2015; revised 25 Sep 2015; accepted 26 Sep 2015; published 1 Oct 2015

Table 3. Fitted parameter values for α-p and α-s measurements from Ag NPs on flat Al_2O_3. Estimated errors are given in parenthesis.

Sample		***x*-azimuth**	***y*-azimuth**
Ag on flat Al_2O_3	A	311(1)	287(2)
	B	62(3)	60(1)
	C	0	0
	F	0	0
	G	-7(1)	-8(1)
	H	138(1)	118(1)

4.1.2. Ag on faceted Al_2O_3:

Figure 5 shows the α–p and α–s response from aligned Ag NPs on faceted sapphire. The polar plots from each azimuth now differ dramatically, with the α–px plot showing lobes rotated by 90° from the isotropic response. Bearing in mind that α is defined with respect to the plane of incidence, both α–p plots show a dominant SH response in the *y* direction along the array. SHG in this off–normal geometry is clearly extremely sensitive to the morphology of the NP layer. It has been shown previously that deposition on the faceted substrate produces truncated ellipsoidal NPs distributed in arrays at the facets, together with some small isotropic NPs on the terraces, as shown in Fig. 1(a) [7, 16]. Figure 5 shows that the anisotropic NP response

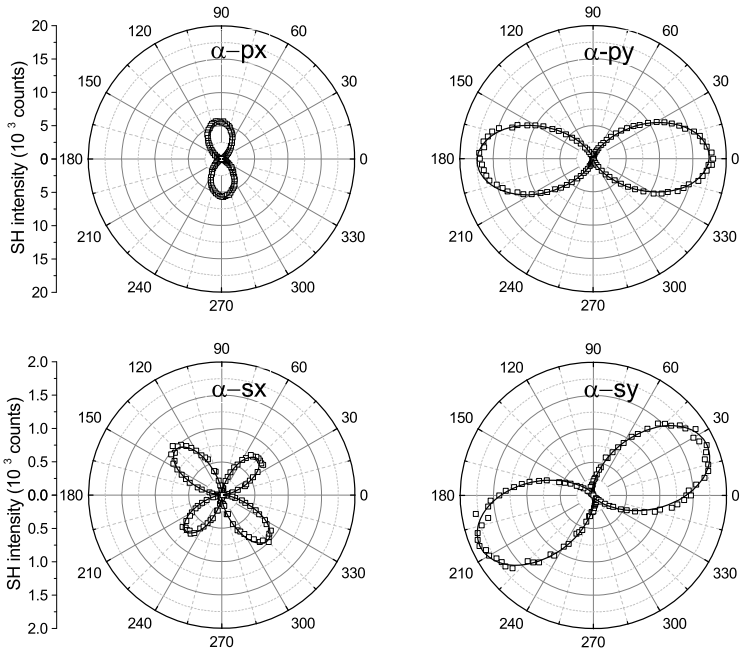

Fig. 5. α–p and α–s SH response plotted as a function of polarizer angle along both azimuths, for Ag NPs on faceted Al_2O_3 together with fits (black line) using Eqs. 1 and 2. Note the change of scale by a factor of 10 in the α-s measurements. The NP arrays are aligned along the *y*–azimuth

#243962 Received 8 Jul 2015; revised 25 Sep 2015; accepted 26 Sep 2015; published 1 Oct 2015

Table 4. Fitted parameter values for α-p and α-s measurements from Ag NPs on faceted Al_2O_3. Estimated errors are given in parenthesis.

Sample		***x*-azimuth**	***y*-azimuth**
Ag on faceted sapphire	A	12(1)	132(1)
	B	76(1)	11(2)
	C	0	0
	F	0	38(1)
	G	$-6(1)e^{i51}$	11(1)
	H	29(1)	12(1)

dominates. The maximum of the α–p response is roughly 3 times larger along the *y*–azimuth than the *x*–azimuth, which is consistent with the higher NP density in the *yz*–plane (see Fig. 1). In addition, Table 1 shows an average spacing between NPs in the *y* direction of 6 nm, a separation where dipole–dipole interactions will have a significant effect on the local fields [18]. Table 1 also shows a NP aspect ratio of 1.2 and thus aligned NPs with an average 20% departure from isotropy in the *y* direction, combined with the dipole–dipole interaction between the NPs in arrays aligned in the same direction, produce the dramatic change in the SH response observed. These results are consistent with recent theoretical work emphasizing the sensitivity of SHG to NP shape [26].

The $|A/B|$ ratio for the *x*–azimuth, across the aligned arrays, appears to be promising as a quantitative measure. From Table 3, this ratio is 5.0 for the isotropic morphology, while from Table 4 this ratio is 0.16, a dramatic change of a factor of 30. Table 2 helps in interpreting these results. The *A* parameter can include up to 6 tensor components, with the isotropic *zzz* component often dominating the interface response. This is not the case here, because the factor of 10 change in the *A* parameter in Table 4 between the $x-$ and $y-$ azimuths shows that *zzz* can make only a small contribution. The larger response from out–of–plane, $z-$ dependent tensor elements allows the *zyy* component of the *B* parameter for the $x-$ azimuth to be identified as the dominant term, the minor component being *xyy*. For the $y-$ azimuth, the *zyy* component appears in the *A* parameter (Table 2), which is very large (Table 4). Normal incidence geometry, as used in SHG microscopy, does not allow access to the $|A/B|$ ratio.

The dominance of the *zyy* component is consistent with stronger local fields along the $y-$ azimuth, where the NPs are closely packed, combined with the larger susceptibility normal to the surface. The $|A/B|$ ratio for the *x*–azimuth is related to the relative strengths of the local field in the $x-$ and $y-$ directions, which in turn depends on the in-plane aspect ratio of the NPs and also the dipole-dipole coupling, if the NPs are closely spaced. The equivalent ratio for the $s-$ polarized SH output involves much smaller quantities. However, the α-s response from each azimuth, although roughly an order of magnitude smaller, is also highly anisotropic. The *x*–azimuth response looks similar to the α–s response from the flat substrate. As discussed above, if the *xz*–plane were a mirror plane of the surface, a simple $\sin^2(2\alpha)$ response would be measured. Figure 5 shows that the *xz*–plane of the NP arrays approximates to a mirror plane, with lobes at 45° and related angles. The very large departure from this behaviour for the *y*–azimuth is consistent with the removal of the *yz* mirror plane due to the faceting and subsequent growth of aligned NPs decorating the facets. Absolute values of *A*–*F* are lower than for the NPs on the flat substrate, because the coverage is significantly less (see Fig. 1(a) and Table 1). Finally, there is only one complex parameter value in Table 4, supporting the argument that the SH response is not significantly resonantly enhanced at the fundamental and SH wavelengths.

The results show that SHG is sensitive to these anisotropic local fields and can identify anisotropy in NP shape and distribution. A simple pP measurement along the two azimuths measures the *A* parameter and is sufficient to identify NP anisotropy, while rotating the input

#243962 Received 8 Jul 2015; revised 25 Sep 2015; accepted 26 Sep 2015; published 1 Oct 2015

polarization gives access to the $|A/B|$ ratio, corresponding to the ratio of pP to sP SH field strengths, which may provide quantitative information (see below). An α–s scan along each azimuth can detect the presence of mirror plane symmetry in the NP response. The α–s results are consistent with previous polarized SHG microscopy at normal incidence, [23–25].

4.2. Ag on rippled Si(001)

Figure 6 shows polar plots of the α–p and α–s response of the rippled nanostructures with arrays of Ag NPs of varying aspect ratio (Table 1), and Table 5 and 6 show the parameter values extracted from the fits. A detailed study of the SHG response from the native–oxide–covered rippled Si(001) substrate at this excitation wavelength has been published previously [37]. The rippled Si(001) response is comparable in size to that of native–oxide–covered Si(001), while

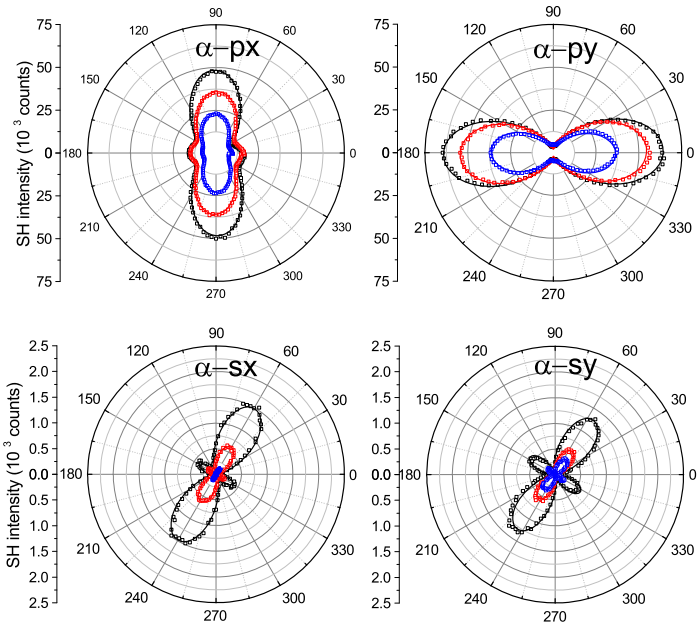

Fig. 6. SH response of capped Ag on rippled Si substrates from both *x* and *y* azimuths plotted as a function of polarizer angle, with fits to Eqs. 1 and 2. Samples S1 (black), S2 (red) and S3 (blue) contain islands of aspect ratio 1.75, 1.60 and 1.47, respectively. Note the change of scale by a factor of 30 in the α-s measurements. The NP arrays are aligned along the *y*–azimuth

the NP response is roughly two to five times larger at these NP densities (Table 1). Thus, in contrast to the faceted Al_2O_3 substrate, there will be a small contribution from the rippled substrate in the response. Figure 6 shows that the NP response is highly anisotropic, with each azimuth being similar in shape to that of NP response on faceted Al_2O_3, see Fig. 5. There is a small but significant difference in the p–x plot in Fig. 6 around $\alpha \sim 0^\circ$ and $\sim 180^\circ$, where small lobes can be seen. Comparison of Table 4 and Table 5 shows that the *A* parameter for the *x*–azimuth has increased in size and has changed sign, relative to the *B* parameter. The overall size of the signal from each azimuth is now similar, reflecting the comparable NP density in each direction, in contrast to the faceted sample, as shown in Fig. 1. The change in the *A* parameter

#243962 Received 8 Jul 2015; revised 25 Sep 2015; accepted 26 Sep 2015; published 1 Oct 2015

Table 5. Fitted parameter values for α-p measurements from Ag NPs on rippled Si. Estimated errors are given in parenthesis.

Sample		*x*-**azimuth**	*y*-**azimuth**
S1	A	-52(5)	246(2)
	B	188(1)	0
	C	0	0
S2	A	-45(4)	237(2)
	B	152(1)	10(5)
	C	0	0
S3	A	-15(4)	184(2)
	B	122(1)	0
	C	0	0

is consistent with the increase in the NP density in the *x* direction, as the tensor components of *A* depend on *x* and *z* fields only.

Overall, the SHG response increases with increasing NP aspect ratio in both directions, S1 having the largest aspect ratio and S3 having the smallest. The general similarity to the faceted results is further evidence for the SHG response being sensitive to anisotropic local fields. This is useful qualitative information, but the number of samples is too small and the variation in the NP size too large to provide definitive quantitative information. For example, the spacing between NPs in the *x* and *y* directions is 15 ± 1 nm and 5 ± 1 nm, respectively, for all three samples (Table 1), indicating that the influence of dipolar coupling between NPs should be similar and leaving the NP aspect ratio as the main difference to be explored. As discussed above, the $|A/B|$ ratio for the *x*–azimuth (across the arrays) is promising as a quantitative measure and values of 0.28(3), 0.30(3) and 0.12(3) for S1, S2 and S3, respectively, are obtained (Table 5). While S3 is clearly distinguished as having the smallest $|A/B|$ ratio, consistent with having the smallest aspect ratio, S1 and S2 cannot be distinguished within error due to the dispersion in NP size.

Turning now to the $s-$polarized SH response, as with the α–p measurements the NPs with larger aspect ratios give larger responses in both directions. There is a clear departure from mirror plane symmetry along both azimuths, as shown by the large values of the *G* parameter and the rotation of the lobes away from 45° and related angles. The contrast between the s–*x* response for the faceted substrate shown in Fig. 5 and the rippled substrate shown in Fig. 6 shows that the $s-$polarized SH response provides qualitative information on the departure from mirror plane symmetry in these NP arrays. The more dominant *H* parameter in the Al_2O_3 sample is consistent with the high quality facets having minimal "snaking" compared to the rippled Si samples.

5. Conclusion

These exploratory *ex situ* studies have shown that the sensitivity of SHG to local fields makes it a promising fixed wavelength characterization technique for anisotropic NP arrays grown by self–assembly. The anisotropic SH response using off–normal geometry is easily detected under non–resonant conditions, avoiding the complexity and expense of spectroscopic SHG. Out–of–plane nonlinear susceptibilities produce SHG intensities an order of magnitude larger than the in–surface–plane response measured using normal incidence, for example in SHG microscopy. Measurements along and across the NP array directions show dramatic differences compared to the SH response of isotropic NPs grown on a flat surface. A simple pP measurement along the two azimuths is sufficient to identify anisotropy in the NP morphology, while measuring the $s-$polarized SH output along each azimuth as the input polarization is rotated can detect

#243962 Received 8 Jul 2015; revised 25 Sep 2015; accepted 26 Sep 2015; published 1 Oct 2015

Table 6. Fitted parameter values for α-s measurements from Ag NPs on rippled Si. Estimated errors are given in parenthesis.

Sample		*x*-azimuth	*y*-azimuth
S1	F	0	0
	G	20(1)	12(1)
	H	26(1)	28(1)
S2	F	0	0
	G	11(1)	12(1)
	H	18(1)	17(1)
S3	F	0	0
	G	6(1)	6(1)
	H	8(1)	16(1)

departure from mirror plane symmetry. By choosing the plane of incidence orthogonal to the NP array direction, it was shown that the $p-$polarized SH response, as a function of input polarization, is very sensitive to NP morphology, with a change of 20% in the inplane aspect ratio of the NPs producing a variation of a factor of 30 in the ratio of the easily measureable pP to sP SH field strengths. The results show that a simple fixed geometry could be used for the *in situ* characterization of anisotropic nanostructure morphology during growth by self–assembly, which could be particularly useful in situations where rotating the sample may be neither desirable nor easily accomplished. While linear optical techniques, particularly RAS [7, 16], are likely to remain the preferred choice for *in situ* NP growth monitoring in real time, these results indicate that SHG is promising as a complementary technique.

Acknowledgments

This work has been funded by Science Foundation Ireland, contract nos 06/IN.1/I91 and 11/RFP.1/PHY/3047, the Irish Research Council for Science, Engineering and Technology (IRCSET), and conducted under the framework of the INSPIRE programme, funded by the Irish Government Programme for Research in Third Level Institutions, Cycle 4, National Development Plan 2007-013. Funding from the Deutsche Forschungsgemeinschaft (DFG FOR 845) is gratefully acknowledged.

#243962 Received 8 Jul 2015; revised 25 Sep 2015; accepted 26 Sep 2015; published 1 Oct 2015